ELSEVIER

Polymer 40 (1999) 7373–7385

polymer

Solid state structure and melting behavior of interdiffused polyethylenes in microlayers

T. Schuman[a], S. Nazarenko[a], E.V. Stepanov[a], S.N. Magonov[b], A. Hiltner[a,*], E. Baer[a]

[a]*Department of Macromolecular Science and Center for Applied Polymer Research, Case Western Reserve University, Cleveland, OH 44106-7202, USA*
[b]*Digital Instruments Inc., 112 Robin Hill Road, Santa Barbara, CA 93117, USA*

Received 13 November 1998; accepted 21 December 1998

Abstract

Gradient structures, produced by interdiffusion in microlayers of a high density polyethylene/linear low density polyethylene polymer pair that cocrystallizes isomorphically, were studied experimentally. Microlayers were taken into the melt for a period of time, and the compositional gradient was fixed by crystallization upon quenching. High specific interfacial area of microlayers offset the low diffusion mobility of polymeric chains so that the microlayer in the melt approached compositional homogeneity on a laboratory time scale. Taking advantage of the systematic change of the melting temperature with the blend composition, the compositional gradient was visualized by progressively melting the microlayer with increasing temperature. This made it possible to monitor the kinetics of interdiffusion without using a chemical label. The compositional profiles were analyzed with a diffusion model formulated for a polydisperse system. Diffusion coefficients for lightly branched and linear polyethylene chains, which correlated well with the data of previous studies, were obtained. It was found that the interlayer boundaries remained stationary during a characteristic time of interdiffusion of the component main fractions, and moved at long times as high molecular weight fractions became involved in interdiffusion. The moving boundary phenomenon was investigated with optical and atomic force microscopy and the development of crystalline morphology in the microscopic compositional gradient was described.

Keywords: Interdiffusion; Microlayers; Microlayer coextrusion

1. Introduction

Coextrusion processes that make the formation of two (or more) polymers into microlayered arrays with hundreds, sometimes thousands, of alternating layers possible, exists [1,2]. The thickness of individual layers in these arrays is of the order of microns or less. The stringent flow conditions required for microlayer coextrusion provide a rare opportunity to combine miscible polymers on a small scale with little or no mixing [3–5]. Heating into the melt state activates interdiffusion and the system gradually converts into a periodic gradient blend with compositional maxima and minima located at the centers of the initial layers. Although the diffusion coefficients of the polymer chains are extremely low, the micron size scale of the microlayers ensures significant compositional changes on the time scale of minutes or hours.

Several examples illustrate how the large surface area of microlayers has been exploited to create gradient structures by interdiffusion of miscible polymers [3–6]. Most recently, the kinetics of interdiffusion of a miscible polymer pair, high density polyethylene (HDPE) and linear low density polyethylene (LLDPE), was studied experimentally in microlayers in order to characterize the conditions required to construct gradient morphologies [6]. Microlayers were taken into the melt for a period of time and the compositional gradient was fixed by crystallization upon quenching. Systematic changes in the melting behavior made it possible to quantify the progress of interdiffusion. The DSC thermograms were analyzed by applying a diffusion model formulated for a polydisperse system. The analysis revealed the role of different fractions and enabled extraction of diffusion coefficients for elementary chains.

The present study continues the characterization of the gradient structures produced by interdiffusion of HDPE and LLDPE in microlayers. A compositional gradient is created by taking the microlayers into the melt and the gradient is fixed subsequently by rapid crystallization. This polymer

* Corresponding author. Tel.: + 001-216-368-4186; fax: + 001-216-368-6329.
E-mail address: pah6@po.cwru.edu (A. Hiltner)

0032-3861/99/$ - see front matter
PII: S0032-3861(99)00013-0

pair cocrystallizes isomorphically, i.e. crystallinity changes linearly between the LLDPE and HDPE values, and the single melting temperature monotonically increases with concentration of HDPE in the blend [7–12]. Hence, as the gradient microlayer is heated into the melting range, melting begins in the LLDPE-rich area and gradually spreads into areas of higher HDPE content as the temperature is increased. This makes it possible to visualize the composition gradient in terms of the melting temperature profile near the layer boundaries. The local melting profile is used in the present study to monitor the kinetics of interdiffusion. The results are correlated with the evolution of the layer structure and with crystalline morphology of the partially interdiffused layers as probed with optical microscopy (OM) and atomic force microscopy (AFM).

2. Experimental

An HDPE and an LLDPE resin were provided by BP Chemicals, Ltd. The HDPE had a density of 0.956 g/cm^3, molecular weight M_w of 316 600 g/mol, and polydispersity of 15.7. The LLDPE comonomer was butene and the ethyl branch content was 20/1000 carbons. The LLDPE had a density of 0.922 g/cm^3, molecular weight M_w of 118 000 g/mol, and polydispersity of 4.2. The molecular weight distributions were provided by the manufacturer [6].

Microlayers with 32 alternating layers of HDPE and LLDPE were extruded as a tape, about 1 mm thick and 0.8 cm wide using the microlayer coextrusion system [1,2] and coextrusion conditions [6] described previously. The viscosity mismatch resulted in some layer non-uniformity. As the lower viscosity LLDPE tended to encapsulate the edges, specimens for analysis were taken from the center of the tape where the average composition was LLDPE:HDPE (40:60 w/w). The average layer thicknesses were 17 and 25 μm for the LLDPE and HDPE layers, respectively; the layer thickness distribution has been described previously [6]. In addition, a microlayer control with 32 LLDPE layers was also prepared.

A 6.6 mm circular disc was stamped from the center of the microlayer tape. Specimens of this size fit snugly into the aluminum sample pan of the Perkin–Elmer DSC-7 and did not get distorted when melted. The pan lid was aligned with the extrusion direction to preserve sample orientation. The temperature of the specimen was raised to 200°C at a heating rate of 200°C/min, held at 200°C for the desired time up to 10 000 min, and cooled at a rate of 40°C/min. Zero minutes indicates that the specimen was raised to 200°C and cooled immediately.

The melt-treated specimen was removed from the DSC pan and halved normal to the extrusion direction. One of the halves was used for thermal analysis and the heating thermogram was obtained with a heating rate of 10°C/min. The other half was used for OM. Sections of about 10 μm thickness were microtomed from the entire cross-section with a cryogenic ultramicrotome. The crystalline morphology was viewed with transmission polarized light microscopy and Nomarski reflection OM.

AFM was performed on the microtomed surfaces with a Nanoscope IIIa (Digital Instruments, Santa Barbara, CA) with the MultiMode head and J-scanner which allows imaging of surface areas as large as 120 × 120 μm^2. The tapping mode [13] was used at ambient conditions. Commercial Si probes with cantilevers 225 μm in length and 5–10 nm probe tips were chosen. The resonance frequencies of these probes were in the 150–170 kHz range. Height and phase images were recorded simultaneously. Height images are primarily related to surface topography, with brighter patterns corresponding to more elevated surface regions. In addition to a top-view presentation, height images are shown as three-dimensional surface plots. Phase images describe changes between the phase of a free-oscillating probe and the probe interacting with the sample surface. On homogeneous materials, phase images provide a more pronounced contrast for morphological features than height images due to the high sensitivity of phase changes to surface imperfections (edges, steps, etc.). Phase images for heterogeneous materials often reflect differences in the mechanical or adhesive properties of individual components, and are extremely useful for compositional mapping in blends, copolymers, and composites [14]. Imaging of the HDPE/LLDPE microlayers was conducted in conditions of *hard* tapping (AFM operation with a large free-oscillation amplitude, A_0, and set-point amplitude of about half of A_0); the differences in the phase images are mostly related to differences in local mechanical properties [15].

To obtain the melting temperature profile, a microtomed section was constrained between a microscope slide and a cover slip, and heated on a Mettler hot stage at a rate of 10°C/min under polarized light. The microscope images were recorded with a video camera. Melting was observed as fading of the birefringence to black. Melting began in the center of the LLDPE layer, progressed through the LLDPE–HDPE interface, and concluded with the center region of the HDPE layer. All the specimens were prepared from the same microlayer tape. The same three-layer sequence (HDPE–LLDPE–HDPE) was analyzed in each specimen. The initial thickness of each layer was determined before the specimen was melted. The average thickness of the melted region was obtained from image analysis of captured video frames by calculating the melted area, and then dividing by the length of the region analyzed. The average position of the melt front from the center of the LLDPE layer was defined as half of the melted region thickness. The position of the melt front was normalized to the length of a periodic element L_0 which consisted of half of an LLDPE layer with half of an adjacent HDPE layer. A plot of the hot stage temperature versus position of the melt front represented the local melting temperature profile.

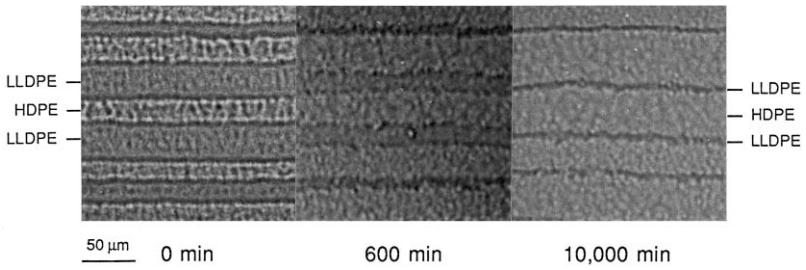

Fig. 1. Optical micrographs of the layers after the microlayer was taken to 200°C for the time indicated.

3. Results and discussion

3.1. Layer structure

Optical micrographs of sections cut from the microlayer after it was in the melt at 200°C are shown in Fig. 1. The layers were easily distinguished at this magnification even after a very long time in the melt. Although the contrast after 600 min was not as strong as initially, the layers were again prominent after 10 000 min. The layer thicknesses remained unchanged if the melt time was less than about 100 min, however, after 600 min in the melt the LLDPE layers were noticeably thinner and the HDPE layers thicker. After 10 000 min, the wavy LLDPE layers became so thin that the total number of layers appeared to have halved from 32 to 16.

The average HDPE and LLDPE layer thicknesses as a function of time in the melt are plotted in Fig. 2. The error bars refer to the deviation among different specimens cut along the length of the microlayer tape. After about 100 min in the melt, perceptible movement of the boundaries in the direction of the faster diffusing component provided evidence of convective flow similar to the Kirkendall effect in metals. This occurs when highly mobile chains diffuse into the region of less mobile chains; the resulting osmotic pressure drives the bulk flow. The effect is most easily observed in polymers if the two components are monodisperse and widely differing in molecular weight [16,17]. Figs. 1 and 2 show that the effect can also be observed in polymers of conventional molecular weight and molecular weight distribution. The LLDPE and HDPE used in this study differed in average molecular weight and polydispersity sufficiently, that domination of the diffusion kinetics by the more mobile LLDPE component was manifest. However, the mismatch of the component diffusional fluxes across the interface appeared only at longer times which corresponded to diffusion of high molecular weight fractions.

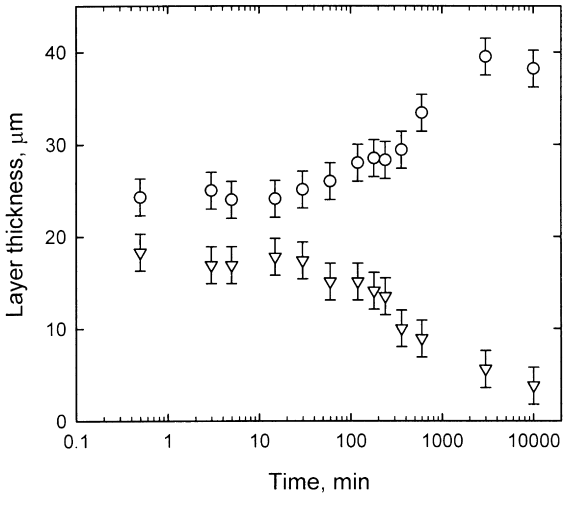

Fig. 2. Change in the average HDPE (circles) and LLDPE (triangles) layer thickness with time at 200°C.

Layers were also revealed in AFM phase images even after the microlayer had been in the melt for 10 000 min (Fig. 3). Qualitatively, the phase images confirmed the gradual change in layer thickness that was detected in optical micrographs (Figs. 1 and 2). The layer boundaries also acquired some waviness that was not present initially. Layer thicknesses in the phase images were generally comparable to those measured from the optical micrographs; however, layer thicknesses for different melt times could not be compared in the AFM phase images because the same part of the microlayer was not imaged at each time period. Data from optical micrographs (Fig. 2) best charted the change in layer thicknesses because they compared the layers taken from the same position in the microlayer at each time period.

In comparison to the phase contrast between LLDPE and HDPE layers, that persisted even after 10 000 min when the microlayer was virtually homogeneous, a microlayer with only LLDPE layers showed a uniform spherulitic texture after 10 000 min at 200°C (Fig. 3(d)). The high resolution possible with AFM revealed the reason for layer definition in AFM phase images, and in polarized optical micrographs, even after very long times in the melt. Submicron holes in the LLDPE layers distinguished the LLDPE layers from the HDPE layers (Fig. 4(a)). Coalescence of the holes in the melt, facilitated by shrinkage of the LLDPE layers, caused the hole size to increase with melt time. After 10 000 min in the melt, which reduced the LLDPE layers to thin, wavy, dark lines, the holes were as large as a micron (Fig. 4(b)).

The absence of submicron holes in the microlayer with only LLDPE layers after 10 000 min at 200°C (Fig. 3(d)) provided confirmation that the holes, which appeared mainly in the LLDPE layers of the HDPE–LLDPE

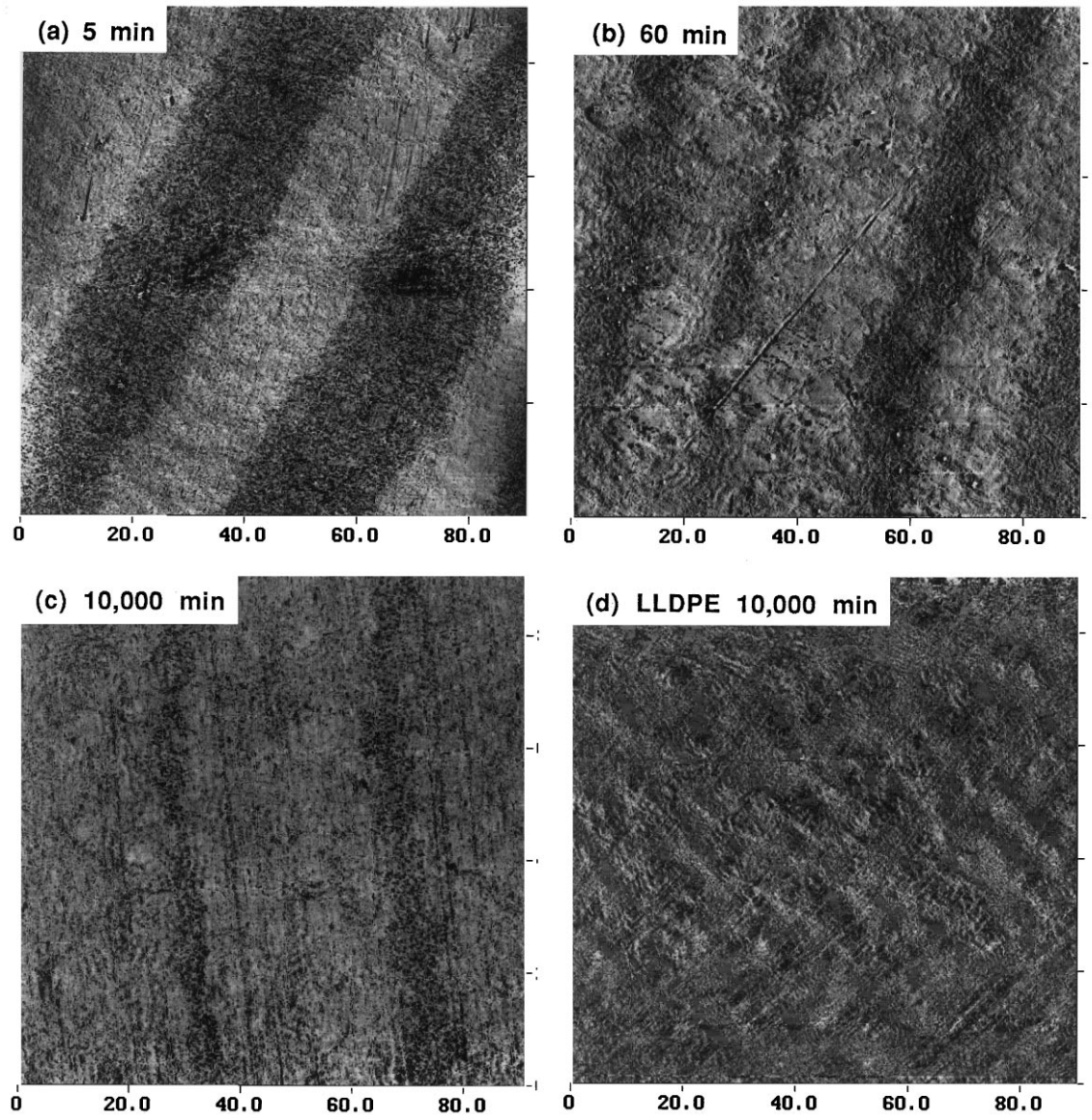

Fig. 3. AFM phase images: the HDPE–LLDPE microlayer after (a) 5 min; (b) 60 min; and (c) 10 000 min at 200°C; compared with (d) the LLDPE microlayer after 10 000 min at 200°C.

microlayer, did not result from degradation of LLDPE. Instead, the holes are thought to originate from the process of microlayering different polymers. Extensional flow through the die elements creates a negative hydrostatic stress component which in turn promotes transient cavitation. Diffusion of dissolved air into the cavities produces an internal pressure that balances the surface tension and prevents the collapse of the cavities. Presumably, this creates stable nucleation sites in both the HDPE and LLDPE layers. Upon cooling from the melt, the HDPE solidifies first. Shrinkage of the HDPE layers produces expansion of the LLDPE layers which are still in the melt. The expansional forces cause the nucleation sites in LLDPE to grow, and the resultant holes freeze upon subsequent crystallization of the LLDPE.

The topology of microtomed surfaces was probed with AFM. The height images (Fig. 5) and corresponding section scans (Fig. 6) show specimens that were at 200°C for different lengths of time. Sharp changes in height at the boundaries between HDPE and LLDPE layers characterize the specimen that was raised to 200°C and cooled immediately (Fig. 5(a)). The corresponding section scan in Fig. 6(a) shows the HDPE layers raised about 300 nm above the LLDPE layers. The stepped topology was also detected when microtomed surfaces were viewed in SEM and in Nomarski reflection OM. Most likely, the topology resulted from residual stresses in the extruded microlayer. As the LLDPE was under hydrostatic tension because of crystallizing after the HDPE, the LLDPE layers contracted when microtoming relieved the stress. Although the layer boundaries gradually lost definition as the time in the melt increased (Figs. 5(b) and 6(b)), the layers remained easily

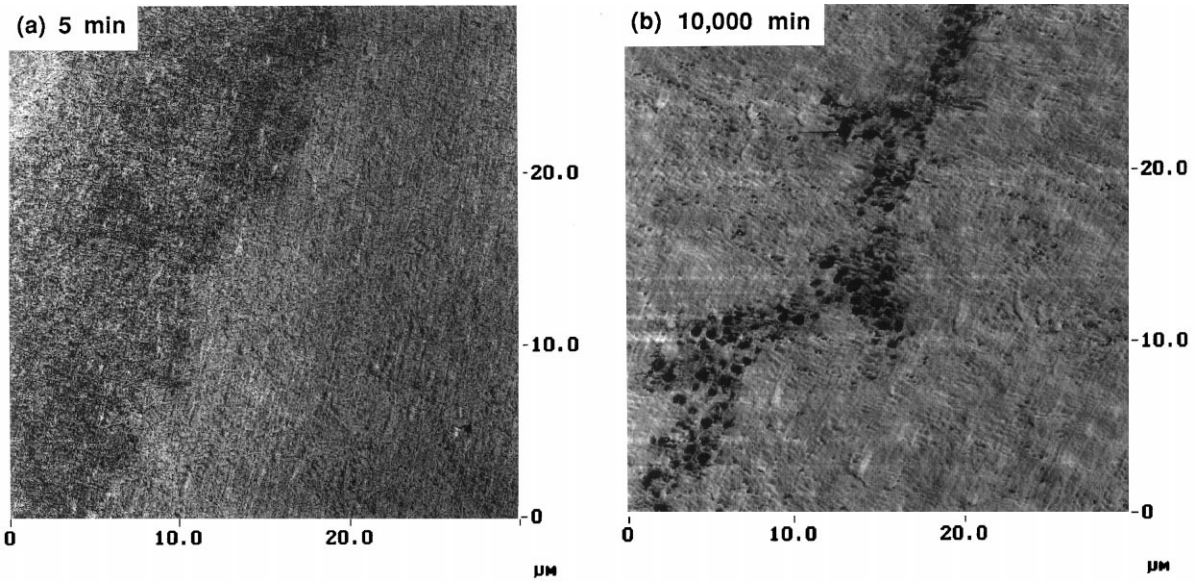

Fig. 4. Higher resolution AFM phase images of the microlayer: after (a) 5 min; and (b) 10 000 min at 200°C.

identifiable even after 60 min in the melt (Figs. 5(c) and 6(c)). The layered topology completely vanished from height images after 3000 min at 200°C (Figs. 5(d) and 6(d)), although the layers remained visible in the OM and AFM phase images. The surface texture of the 3000 min height images arose from the spherulitic morphology.

The reason layers were clearly distinguishable in the OM after either very short or very long times in the melt, and

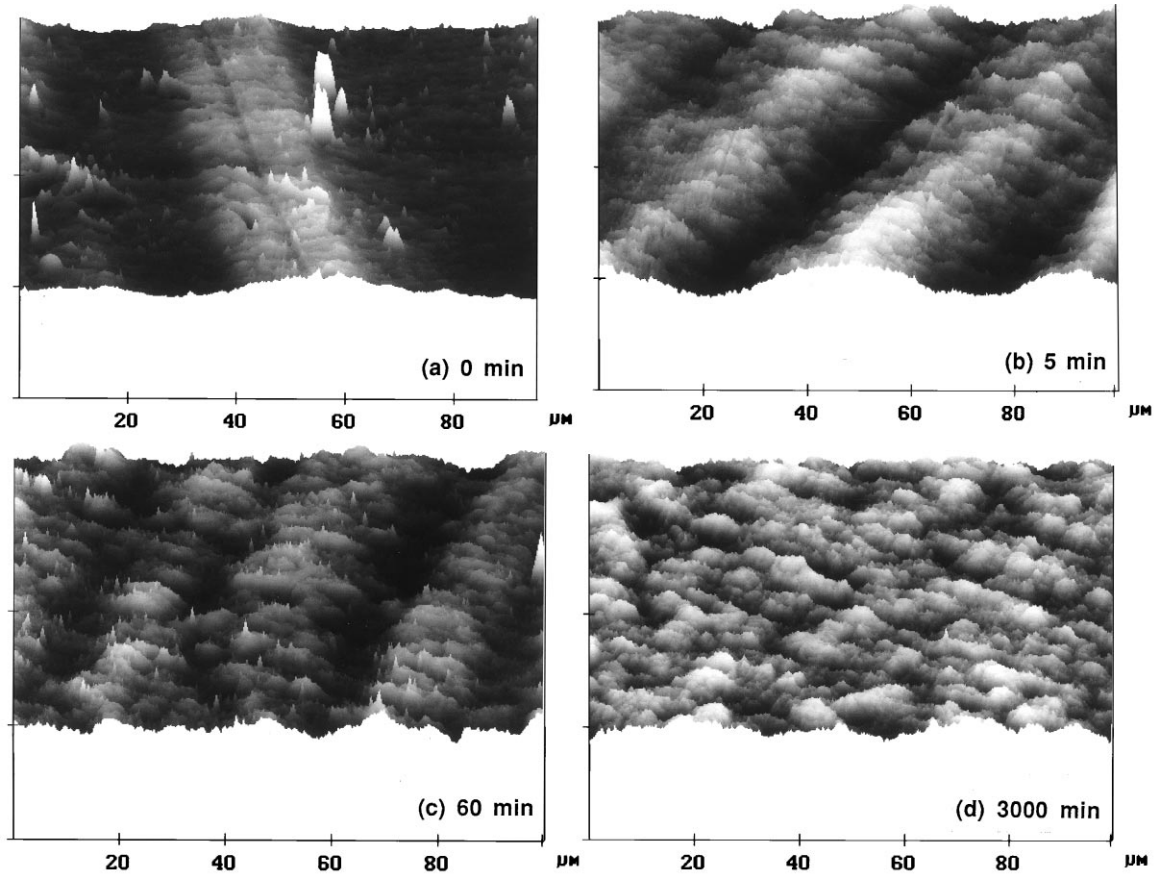

Fig. 5. Three-dimensional AFM height images: after (a) 0 min; (b) 5 min; (c) 60 min; and (d) 3000 min at 200°C.

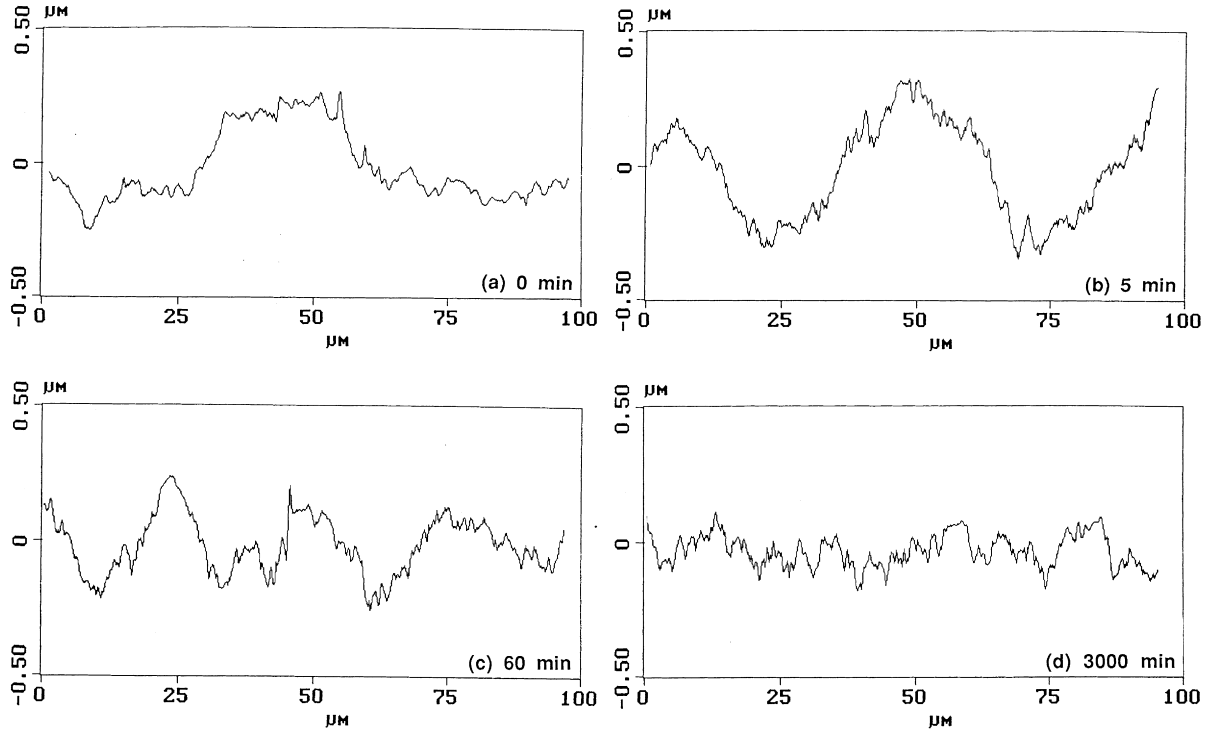

Fig. 6. AFM section analysis of the images in Fig. 3: after (a) 0 min; (b) 5 min; (c) 60 min; and (d) 3000 min at 200°C.

were less clear at intermediate times (e.g. 600 min) was now understandable. Initially the layers were easily visible in the OM because of height and density contrasts, and in the AFM where height and modulus differences provided contrast. As interdiffusion proceeded, these sources of contrast diminished and after several thousand minutes in the melt were completely erased. Fortuitously, the holes in the microlayer acted as markers for the LLDPE layer and made it possible to chart the position of the layer boundary as the composition gradient diminished. Although the submicron holes were initially too small to scatter light efficiently, after several thousand minutes in the melt they coalesced to the micron size and the LLDPE layers were easily visible by scattered light in the OM and by phase contrast in the AFM. The layers were most difficult to distinguish at intermediate times when the topological definition was declining and the hole size was increasing.

The crystalline morphology, as exposed in the polarized light microscope, initially conformed to the layer boundaries (Fig. 7(a)). Space-filling spherulites characterized the HDPE layer; the LLDPE layer consisted of a transcrystalline region immediately adjacent to the HDPE layer with a band of spherulites in the center of the layer. Transcrystallinity requires an interface between materials with different crystalline habits. Not surprisingly, transcrystallization was strongly affected by changes in the composition gradient that occurred early in the interdiffusion process. After 15 min in the melt, the transcrystalline texture was thicker, more irregular, and in places penetrated into the spherulitic HDPE layer; simultaneously, the band of spherulites in the center of the LLDPE layer contracted (Fig. 7(b)). As a result, the layers remained discernable although they were less well-defined than initially. After 105 min at 200°C, transcrystallinity was gone and the layers were not discernable in the overall spherulitic morphology (Fig. 7(c)). Longer times in the melt did not produce any further change.

3.2. Melting behavior

Bulk melting thermograms of the HDPE–LLDPE microlayer initially exhibited two melting peaks with maxima at 123 and 131°C, compared to 122 and 132°C for LLDPE and HDPE with the same process and thermal history. This confirmed minimal mixing of the two polyethylenes during coextrusion. A series of thermograms in Fig. 8 shows the effect of residence time at 200°C on the melting behavior of the microlayer. The gradual convergence of the two melting peaks toward a single peak as the time increased reflected the progress of interdiffusion. A single peak was first observed after about 100 min at 200°C. Additional time in the melt produced virtually no change in the melting temperature, but served to sharpen the peak. The peak shape approached that of a melt blend with the same composition only after about 600 min at 200°C.

Changes that occurred in the first 100 min, notably the appearance of a uniform spherulitic texture and a single melting peak, established that most of the material interdiffused in this time period before there was any significant movement of the boundary. It follows that the high molecular weight fraction that drives the Kirkendall effect of a

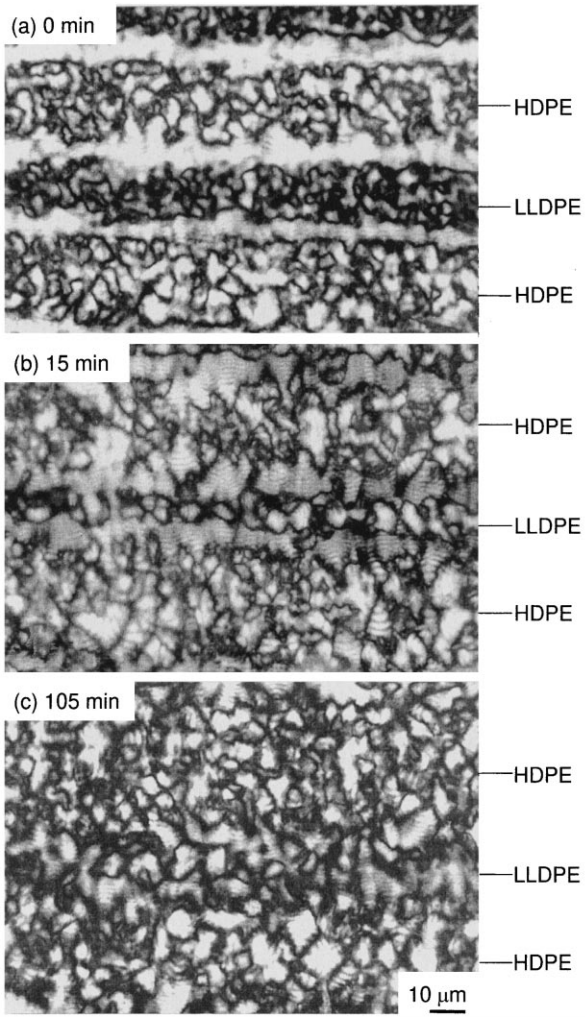

Fig. 7. Polarized light micrographs of the microlayer: after (a) 0 min; (b) 15 min; and (c) 105 min at 200°C.

moving boundary is very small. This validated the assumption, used previously in the analysis of the bulk melting behavior [6], that the boundary remains stationary during the characteristic interdiffusion time of the major fractions of both components. Despite the small contribution to the total mass, the long chain entanglement network sustained the residual stresses. These stresses were responsible for the surface topology, which persisted even after 60 min in the melt, and for cavitation of the LLDPE layers.

Direct observation of the melting profile was made on the hot stage. The two series of polarized light micrographs in Fig. 9 compare the melting of microlayers that had been at 200°C for 0 and 60 min. In the microlayer that had been at 200°C for 0 min, fading of the LLDPE layers at 122°C suggested that they had started to melt; at 125°C the LLDPE layers were completely melted; there was no visible change at 128°C; and at 131°C the HDPE layers were faded but not completely melted. In the microlayer that had been at 200°C for 60 min, the LLDPE layers had not started to melt at 122°C; they were partially melted at 125°C; at 128°C, the LLDPE layers were completely melted and a noticeable thinning of the HDPE layers indicated that the melting front had progressed across the interface; and at 131°C the HDPE layers had completely melted. Narrowing of the melting range due to the composition gradient produced by interdiffusion was most apparent by comparing the images at 122 and 131°C. The LLDPE layers started to melt at a higher temperature, and the melting of the HDPE layers was complete at a lower temperature, in the microlayer that had been at 200°C for 60 min compared to the microlayer that had been at 200°C for 0 min.

The melting temperature profiles after various time intervals in the melt at 200°C are depicted in Fig. 10. On each plot, the first experimental point lies some distance from the origin, i.e. from the center of the LLDPE layer. This defines the thickness of the field within the LLDPE layer that melted instantly upon reaching the lowest temperature. Similarly, the last experimental point defines the field within the HDPE layer that melted at once as the highest temperature was achieved.

The profiles were well resolved for comparatively short times in the melt, 5 and 15 min (Fig. 10(a) and (b)). As the temperature of the hot stage increased through the melting range, the melt boundary remained quite sharp and the position of the melt front could be unambiguously determined. For 60 and 90 min (Fig. 10(c) and (d)), there was more uncertainty in the measurements as the boundary between the melt and solid became more tortuous and diffuse. With further increase in the time at 200°C, the gradient in melting temperature diminished, but did not vanish entirely. Even after a week at 200°C, there was a 2°C melting gradient across the microlayer. However, due to noticeable shrinkage of the LLDPE layers and increasing subjectivity in the image analysis, the long melt time data were considered only qualitatively.

3.3. Diffusion model for the polydisperse system

Evolution of the melting temperature profile with time reflected the progress of interdiffusion. The melting temperature can be correlated with the local component composition by utilizing the data on melt blends of the same HDPE–LLDPE pair (Fig. 11). Thus, the composition profile, as represented by the melting temperature profile, gradually flattened out with increasing interdiffusion time. By analyzing the data with the interdiffusion model developed previously [6], it was possible to determine the parameters that control the homogenization kinetics.

Modeling the progress of interdiffusion in a polydisperse system requires consideration of the strong dependence of the diffusion coefficient on the molecular weight. The molecular weight distributions of the LLDPE and HDPE, $G_1(M)$ and $G_2(M)$, are well approximated by normal logarithmic functions that are shown in Fig. 12. As can be seen, the polydispersity is rather high with the fractions spread out over more than two orders of magnitude in molecular

weight, from about 10^4 to higher than 10^6. This means that the time scale of interdiffusion for the fractions can differ in several orders of magnitude. Such a considerable difference obviously affects the net kinetics of interdiffusion.

To account for polydispersity, diffusion of each molecular weight fraction was considered separately. As both the components were polyethylenes, their melt densities and the densities of their blends in the melt were assumed to be the same and independent of molecular weight. Additionally, the interaction parameter could be taken as zero for this system [12]. These assumptions removed from consideration any concentration dependence of the fractional diffusion coefficients. Thus, diffusion of each fraction could be considered as proceeding independently from other fractions of the same component as well as from all fractions of the other component. This is consistent with previous observations that the diffusion coefficient of a monodisperse specie in a polyethylene matrix is not affected by the matrix molecular weight if the latter is 2–3 times higher than the critical entanglement molecular weight [18,19].

Accordingly, the fractional diffusion coefficient was determined by molecular weight only. For this dependence, the ordinary power law was used [18,20,21]:

$$D_{M,i} = D_{0,i}\left(\frac{\bar{M}_i}{M}\right)^{\alpha}, \quad (1)$$

where $D_{M,i}$ is the diffusion coefficient for the fraction of component i with molecular weight M, $\bar{M}_i$, the component i weight average molecular weight, and $D_{0,i}$, the diffusion coefficient of chains of the average molecular weight chosen as a reference. The power α characterizes the sharpness of the molecular weight dependence of the diffusion coefficient, and takes values from 1 to 3 for various systems [18,21]. Values around $\alpha = 2$, which follows from reptation theory [22,23], are commonly reported for diffusion of polyethylenes [19,24–30]. This value is considered for the present analysis.

The net diffusional flux of each component toward the other is determined by summation of the fractional fluxes. As a result of different molecular weight distributions and diffusion coefficients, the net fluxes, in general, will not match each other. Convective flow of the melt compensates for the mass loss and assures the density conservation. Experimentally, convective flow reveals itself by the movement of the interface towards the faster diffusing component [16,17]. For the system under investigation, the shrinkage of LLDPE layers at longer times (Figs. 2 and 5) was an indication of this movement. However, as seen by comparison of Fig. 2 with Fig. 8, the shift was significant only at times longer than 300 min at 200°C, when a single melting peak on the DSC thermogram (Fig. 8) indicated that the components were almost completely intermixed. Thus, the interface could be assumed to be stationary during the characteristic interdiffusion time of the major fractions of both the components. The mismatch of the diffusional fluxes appeared only at the longer time scale corresponding to diffusion of high molecular weight fractions, which represented a small percentage of the total amount of material. As the high molecular weight tail was significantly larger in the HDPE distribution than in the LLDPE distribution, immobility of long HDPE chains at times when the LLDPE concentration had flattened was compensated by convective mass flow of the HDPE layer.

Thus, analysis of concentration profiles at the initial period of interdiffusion can be made with the assumption of a stationary interface. As seen by convergence of the

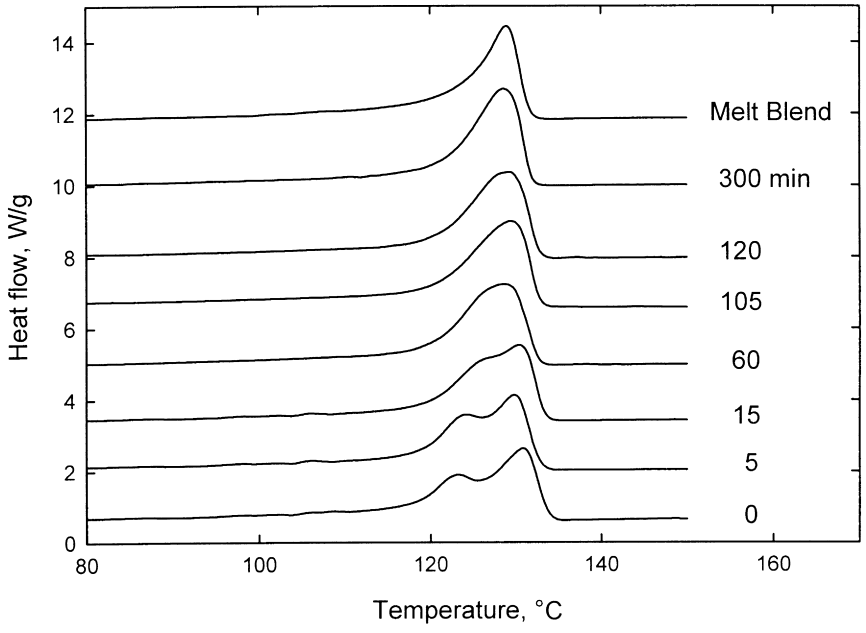

Fig. 8. Melting thermogram of the microlayer after increasing the time at 200°C.

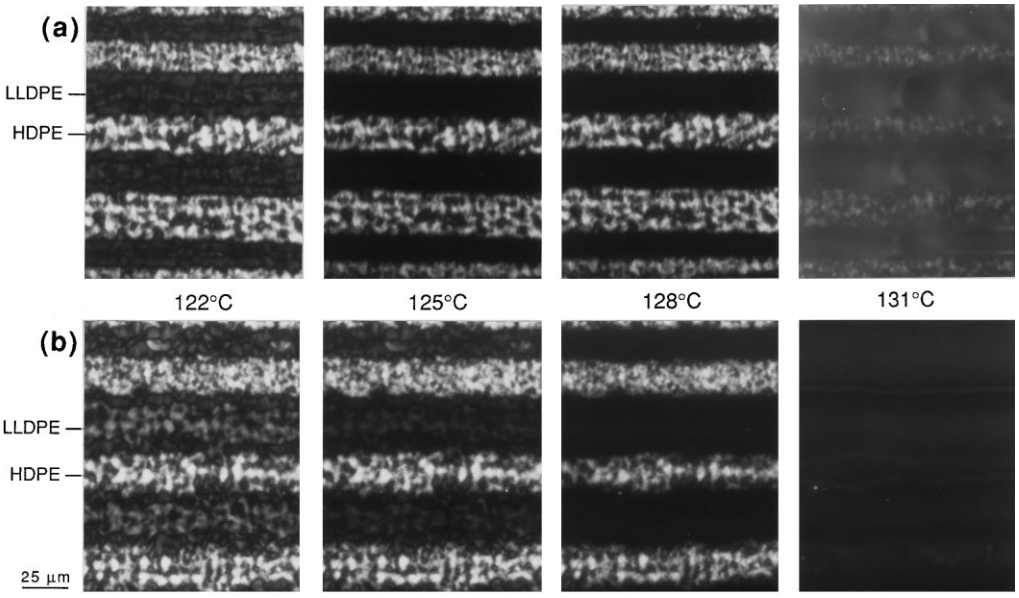

Fig. 9. Polarized light micrographs showing melting of the microlayer: after (a) 0 min; and (b) 60 min at 200°C.

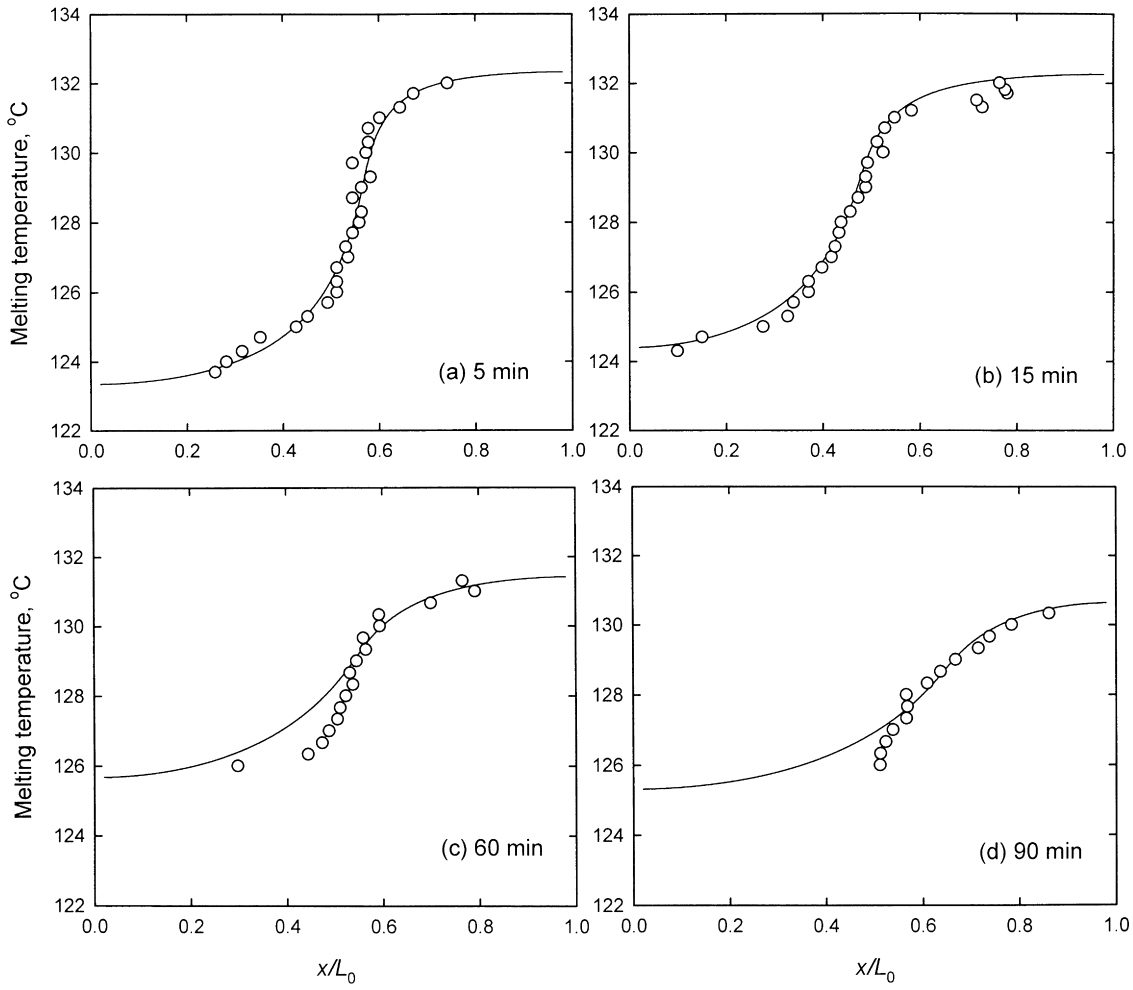

Fig. 10. Experimental melting temperature profiles (open circles) compared with calculated melting temperature profiles (solid lines): after (a) 5 min; (b) 15 min; (c) 60 min; and (d) 90 min at 200°C.

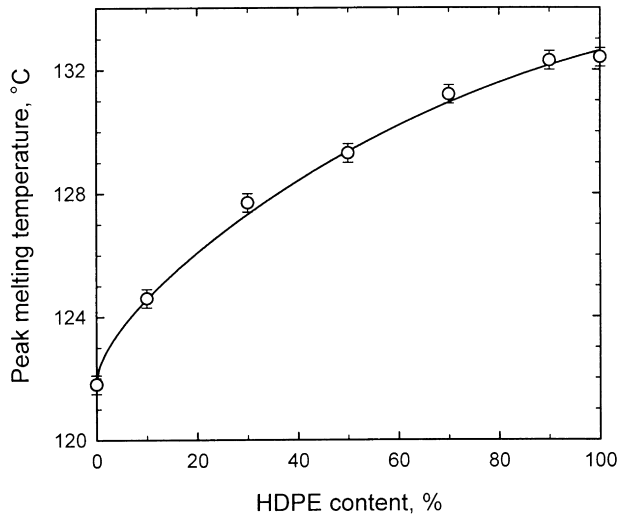

Fig. 11. Dependence of the peak melting temperature on the composition of HDPE–LLDPE melt blends.

melting peaks with increasing interdiffusion time (Fig. 8), the composition changes during the first 100 min enough to provide sufficient information for determining the diffusion coefficients of the components $D_{0,i}$. Having obtained $D_{0,i}$, evolution of the compositional gradient at longer times can be readily understood by comparison of the mass fluxes of higher molecular weight fractions as they gradually became involved in interdiffusion.

For the stationary interface, the fractional concentration distribution is described by the following equation:

$$\frac{\partial w_{M,i}}{\partial t} = D_{M,i}\frac{\partial^2 w_{M,i}}{\partial x^2}, \tag{2}$$

where $i = 1,2$ for LLDPE and HDPE respectively, and $w_{M,i}$ is the weight concentration of the fraction of component i with molecular weight M divided by its initial value $\rho G_i(M)$

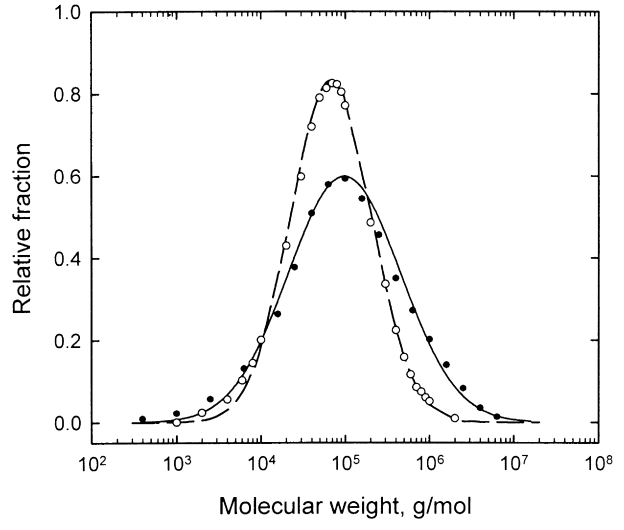

Fig. 12. Molecular weight distributions of LLDPE and HDPE shown as the experimental data (circles) and the Gaussian approximation (lines).

(the density ρ is assumed to be the same for both components). Eq. (2) was solved in the interval of the interdiffusion element $0 < x < L_0$ with initial and boundary conditions that assumed total separation of the components on the interface at L_1 at zero time, and no flux out of the interdiffusion element:

$$w_{M,i}(x, t = 0) = (-1)^i \theta(x - L_1),$$
$$\frac{\partial w_{M,i}}{\partial x}\Big|_{x=0,L_0} = 0, \tag{3}$$

where $\theta(x)$ is the Heaviside's step function. Incorporating the molecular weight dependence given by Eq. (1), the solution of Eq. (2) took the form:

$$w_{M,1}(x,t) = h\left(\frac{L_1}{L_0}, \frac{x}{L_0}, \frac{t}{\tau_{M,1}}\right),$$
$$w_{M,2}(x,t) = h\left(1 - \frac{L_1}{L_0}, 1 - \frac{x}{L_0}, \frac{t}{\tau_{M,2}}\right), \tag{4}$$

where the function

$$h(l, x', t') = l + \sum_{n=1} \frac{2}{n\pi}\sin(n\pi l)\cos(n\pi x')\exp[-n^2 t'] \tag{5}$$

describes the shape of the fractional concentration profile in terms of the dimensionless coordinate x' and time t'; and

$$\tau_{M,i} = \frac{L_0^2}{\pi^2 D_{0,i}}\left(\frac{M}{\bar{M}_i}\right)^{\alpha} \tag{6}$$

represents the characteristic time for diffusion of the fraction. Total concentration profiles are defined by integration over the fractions:

$$W_i(x,t) = \int_M w_{M,i}(x,t) G_i(M)\, \mathrm{d}M \tag{7}$$

and the net diffusional fluxes of the components through the interface are determined by the relationship:

$$J_i(t) = -\rho \int_M D_{M,i}\left[\frac{\partial w_{M,i}}{\partial x}\right]_{x=L_1} G_i(M)\, \mathrm{d}M. \tag{8}$$

The solution, given in Eqs. (4)–(7), is not rigorously consistent with local density conservation $W_1 + W_2 \equiv 1$ if the components are of different polydispersities $G_i(M)$. The same is true even for a weaker condition $J_1 + J_2 = 0$ which describes conservation in density averaged over each layer. Some convective flow must always occur in a polydisperse system. Neglect of this flow is possible only at the specific ratio of the diffusion coefficients $D_{0,i}$ that yields the best match of the component diffusional fluxes. Persistence of a stationary interface determines the time scale over which this assumption is valid for this system. Violation of the local density conservation is also minimized in this way.

To formulate a condition which could replace the exact local density conservation requirement, deviation of the interface from its initial position was minimized over a

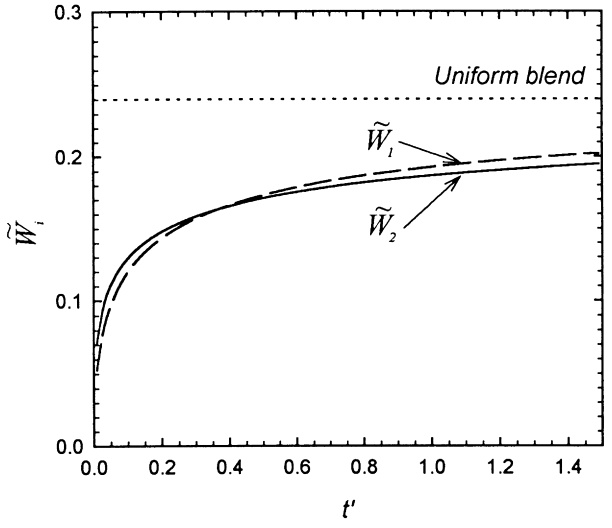

Fig. 13. Normalized amount of HDPE (solid line) and LLDPE (dashed line) that crossed the interface in time t' referred to the characteristic interdiffusion time for the weight average fraction. The dotted line shows the asymptotic value for both the functions corresponding to complete intermixing.

time scale when the stationary interface was observed. As a result of the total flux continuity, the interface velocity $\dot{l}$ is defined by equation:

$$\rho\dot{l} = J_1 + J_2 \tag{9}$$

and the interface shift is determined by the difference $\Delta\bar{W}$ between the quantities:

$$\bar{W}_i(t) = (-1)^{i+1}\frac{1}{\rho}\int_0^t J_i(t')\,\mathrm{d}t' \tag{10}$$

which represents the amount of component i that has crossed the interface from each side in time t. If $\Delta\bar{W}$ is relatively small, Eqs. (4)–(8) can be used to calculate $\bar{W}_i(t)$. In these terms, the condition is formulated as the requirements that the quantity:

$$\int_0^\tau (\bar{W}_1(t) - \bar{W}_2(t))^2\,\mathrm{d}t \tag{11}$$

take a minimum during a time τ of the stability of interface while varying the diffusion coefficients, and $\Delta\bar{W}/\bar{W}_i \ll 1$ when calculated at the minimum. Eq. (11) can be reduced to functions of dimensionless variables by referring the diffusion coefficients and the characteristic time to one of the components: $s = D_{0,2}/D_{0,1}$ and $t' = t/\tau_{0,1}$ where $\tau_{0,1} = L_0^2/\pi^2 D_{0,1}$, and defining $H_1(t') = \bar{W}_1(t'\tau_{0,1})$ and $H_2(st') = \bar{W}_2(t'\tau_{0,1})$. Performing the minimization over s, the condition is formulated as a parametric integral equation:

$$\int_0^\beta (H_1(t') - H_2(st'))(t'J_2(st') - H_2(st'))\,\mathrm{d}t' = 0, \tag{12}$$

where $\beta = \tau/\tau_{0,1}$. The solution of the equation gives the ratio of the diffusion coefficients s which is most consistent with a stationary interface in a polydisperse system.

Eq. (12) was solved numerically with the molecular weight distributions $G_i(M)$ shown in Fig. 12, the exponent $\alpha = 2$, and the interface position equal to the average LLDPE–HDPE composition, $l = 0.4$. The value of β cannot be precisely defined before $D_{0,1}$ is determined. However, having accepted that the interface remained stationary during a characteristic time of interdiffusion of major fractions, as discussed earlier, it was considered that $\beta = 1$. The value $s = 0.48$ was obtained for the ratio between the LLDPE and HDPE weight average fraction diffusion coefficients. Trial calculations with the given functions $G_i(M)$ showed that varying β between 0.5 and 2 changed s only in the second significant digit, and $\beta = 1$ can be considered accurate enough.

Using $s = 0.48$, the dynamics of interdiffusion is shown in Fig. 13 in terms of normalized functions $\tilde{W}_i(t') = \bar{W}_i(t'\tau_{0,1})/L_0$. In accordance with Eq. (9), the difference $\Delta\tilde{W}$ between these functions shows the interface shift relative to the total length of the interdiffusion element. As seen, the curves almost coincide, the difference between them varies within a value of 0.02 (0.5 μm in real length), which is much less than the experimental accuracy (Fig. 2). At times $t' \gg 1$, the curves increasingly diverge so that the amount of HDPE diffused into the LLDPE layer is less than that of LLDPE diffused into the HDPE layer. This causes the interfaces on either side of an LLDPE layer to move toward each other. Thus, the LLDPE layer appears to shrink, in accordance with the experimental observations.

Calculation of the component concentration profiles $W_i(x,t)$ with $s = 0.48$ tested how consistent Eqs. (4)–(7) were with the local density conservation. At $t' < 1$, the identity $W_1 + W_2 \equiv 1$ was fulfilled within a 1–2% accuracy. Fig. 14(a) shows the concentration profile of HDPE, W_2, and the total concentration $W_1 + W_2$ calculated at $t' = 0.5$. To illustrate the effect of polydispersity, the profile is compared with that calculated with the monodisperse model at the same time, assuming that the diffusion coefficient D in the monodisperse model is equal to the diffusion coefficient of the weight average fraction $D_{0,1}$. Comparison for long interdiffusion times ($t' = 5$) is made in Fig. 14(b). At short times, rapid diffusion of the low molecular weight chains is responsible for the more shallow profile in the polydisperse model compared to the simple model. Conversely, the concentration gradient persists at long times in the polydisperse model because diffusion of the high molecular weight chains is very slow. The total concentration profile $W_1 + W_2$ at long times shows a regular trend to rarefaction of the LLDPE layer and densification of the HDPE one, which gives rise to the compensating convective flow toward the LLDPE layer as discussed earlier.

3.4. Description of the melting temperature profile

The model was applied to the experimental data by calculating the concentration distribution according to Eq. (7) and converting the concentration to the melting temperature using the correlation presented in Fig. 11. The LLDPE

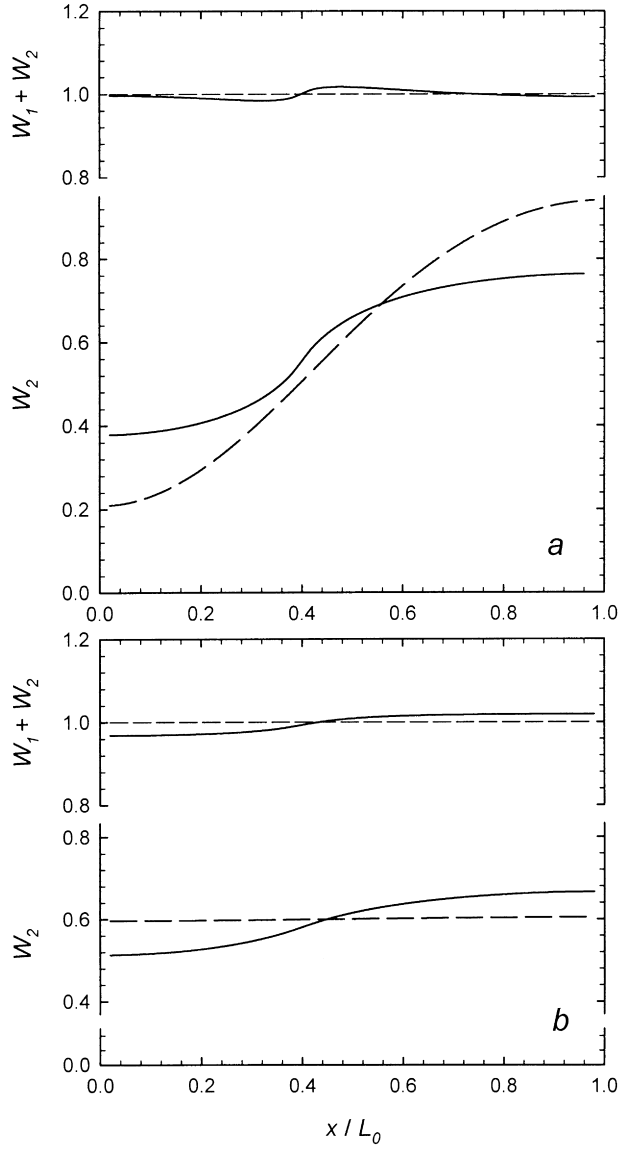

Fig. 14. The HDPE concentration profile over an interdiffusion element, W_2, and the sum of both the component concentrations, $W_1 + W_2$, as calculated by the polydisperse (solid line) and the monodisperse (dashed line) models at (a) short and (b) long times.

Table 1
Diffusion parameters from the melting temperature profiles

Time in the melt (min)	Diffusion coefficient, $D_{0,1}$ (10^{-11} cm^2/s)	Interlayer boundary, l
5	2.1	0.57
5	3.3	0.52
15	2.2	0.48
15	2.9	0.52
60	3.0	0.55
60	2.3	0.65
90	3.8	0.60
90	3.4	0.65

and HDPE concentrations were considered as complimentary to unity with the ratio of the diffusion coefficients $s = 0.48$. The values of $D_{0,1}$ and the interface position $l = L_1/L_0$ were fitting parameters for each set of data. Only data for interdiffusion times less than 100 min, when the boundary was stationary, were analyzed.

As seen in Fig. 10(a) and (b), the model gave an excellent description of data for interdiffusion times of 5 and 15 min at 200°C. The data for 60 and 90 min (Fig. 10(c) and (d)) showed a larger deviation, systematically underestimating the melting temperature distribution in the LLDPE layer. The fit of the latter data was made with an artificial increase of the statistical weight of the edge points as the lowest and highest melting temperatures were the most reliably measured. The results of the fit are presented in Table 1. The value of the reference diffusion coefficient of LLDPE chains, $D_{0,1}$, averaged over all experiments was $D_{0,1} = (2.9 \pm 0.6) \times 10^{-11}$ cm^2/s. Accordingly, the reference diffusion coefficient of the homopolymer was $D_{0,2} = s\ D_{0,1} = (1.5 \pm 0.3) \times 10^{-11}$ cm^2/s. Taking into account the different molecular weight distributions of the interdiffusing components, it is convenient to present the diffusion coefficients in terms of so-called prefactors, defined in accordance with the quadratic molecular weight dependence, Eq. (1), as the ratio D/M^2, where D is the diffusion coefficient for the chains of molecular weight M [18,21]. Thus, the prefactors are equal to 0.40 ± 0.08 cm^2 mol^2/s g^2 for branched LLDPE chains, and 1.5 ± 0.3 cm^2 mol^2/s g^2 for linear HDPE chains. These magnitudes are in good agreement with the values of 0.45 ± 0.07 and 1.6 ± 0.2 cm^2 mol^2/s g^2, respectively, which were obtained previously by the analysis of the bulk melting behavior of the same polymer pair [6]. They also correlate well with direct measurements of the diffusion coefficients of chemically labeled polyethylene chains by NMR, neutron scattering and other techniques, discussed in detail previously [6].

The scatter in the diffusion coefficients obtained in different experiments (Table 1) is thought to be mainly caused by some uncertainty in measurements of layer thicknesses, made at room temperature in crystalline specimens. Upon melting, the thicknesses change due to difference in the crystalline and melt densities, and also because of non-uniform release of residual stresses. As the diffusion coefficient is present in Eq. (4) in combination with L_0^2, Eq. (6), the values of $D_{0,1}$, obtained from the fits were rather sensitive to the variations in L_0.

In summary, we studied interdiffusion and the progress of gradient crystalline morphology in microlayers of polydisperse polyethylenes. We showed that the compositional gradient in partially intermixed microlayers can be visualized by progressively melting the microlayer with increasing temperature. This comparatively simple technique made it possible to monitor kinetics of interdiffusion in the isomorphically cocrystallizing polymer pair. Interdiffusion was significantly affected by polydispersity, so that different fractions participated in the process on different time scales.

However, even though the diffusion coefficient depends strongly on molecular weight, boundary movement was well pronounced only after the main fractions were intermixed. It was caused by relative immobility of a high molecular weight fraction of one of the components. This effect resulted in shrinkage of the layers of the faster diffusing component. During shrinkage, they accumulated morphological defects. Our findings also indicate that time for homogenization of miscible systems depends more on the molecular weight distribution, especially the high molecular weight tail, and less on the dimensions of the phases. This result has implications to the kinetics of heat sealing of polymer films. Overall, the study demonstrates the feasibility of creating gradient morphologies from microlayers on an accessible time scale.

Acknowledgements

This research was generously supported by the National Science Foundation (grant DMR97-05696) and the US Army Research Office (DAAG55-98-1-0311).

References

[1] Mueller CD, Nazarenko S, Ebeling T, Schuman TL, Hiltner A, Baer E. Polym Engng Sci 1997;37:355.
[2] Mueller CD, Ebeling T, Kerns J, Nazarenko S, Hiltner A, Baer E. In: Coates PD, editor. Polymer Process Engineering 97, London: The Institute of Materials, 1997.
[3] Pollock G, Nazarenko S, Hiltner A, Baer E. J Appl Polym Sci 1994;52:163.
[4] Haderski D, Nazarenko S, Hiltner A, Baer E. Macromol Chem Phys 1995;196:2545.
[5] Nazarenko S, Haderski D, Hiltner A, Baer E. Macromol Chem Phys 1995;196:2563.
[6] Schuman T, Stepanov EV, Nazarenko S, Capaccio G, Hiltner A, Baer E. Macromolecules 1998;31:4551.
[7] Hu S-R, Kyu T, Stein S. J Polym Sci: B: Polym Phys 1987;25:71.
[8] Alamo RG, Glaser RH, Mandelkern L. J Polym Sci: B: Polym Phys 1988;26:2169.
[9] Edward GH. British Polym J 1986;18:88.
[10] Hay JN, Zhou X-Q. Polymer 1993;34:2282.
[11] Rhee J, Crist B. Macromolecules 1991;24:5663.
[12] Pracella M, Benedetti E, Galleschi F. Thermochim. Acta 1990;162:163.
[13] Zhong Q, Innis D, Kjoller K, Elings VB. Surf Sci Lett 1993;290: L688.
[14] Magonov SN, Elings V, Whangbo M-H. Surf Sci Lett 1997;375: L385.
[15] Magonov SN, Heaton MG. Am Lab 1998;30:9.
[16] Kramer EJ, Green P, Palmstrom J. Polymer 1984;25:473.
[17] Wu S, Chuang H-K, Han CD. J Polym Sci: B: Polym Phys 1986;24:143.
[18] Kausch HH, Tirrell M. Annu Rev Mater Sci 1989;19:341.
[19] von Seggern J, Klotz S, Cantow H-J. Macromolecules 1991;24: 3300.
[20] Tirrell M. Rubb Chem Technol 1984;57:523.
[21] Green PF. In: Neogi P, editor. Diffusion in polymers, New York: Marcel Dekker, 1996. pp. 251–302.
[22] de Gennes P-G. Scaling concepts in polymer physics. Ithaca: Cornell University Press, 1979.
[23] Doi M, Edwards SF. The theory of polymer dynamics. Oxford: Oxford University Press, 1986.
[24] Bartels CR, Crist B, Graessley WW. Macromolecules 1984;17:2702.
[25] Klein J, Fletcher D, Fetters LJ. Faraday Symp Chem Soc 1983;18:159.
[26] Klein J, Fletcher D, Fetters LJ. Nature 1983;304:526.
[27] Klein J, Briscoe BJ. Proc R Soc Lond A 1979;365:53.
[28] Klein J. Phil Mag A 1981;43:771.
[29] Pearson DS, Ver Strate G, von Meerwall E, Schilling FC. Macromolecules 1987;20:1133.
[30] Bachus R, Kimmich R. Polymer 1983;24:964.